4246–4257 *Nucleic Acids Research, 2022, Vol. 50, No. 8* *Published online 12 April 2022*
https://doi.org/10.1093/nar/gkac245

Visualization of ligand-induced *c-MYC* duplex–quadruplex transition and direct exploration of the altered *c-MYC* DNA-protein interactions in cells

Jia-Hao Yuan, Jia-Li Tu, Guo-Cai Liu, Xiu-Cai Chen, Zhi-Shu Huang, Shuo-Bin Chen* and Jia-Heng Tan*

Guangdong Provincial Key Laboratory of New Drug Design and Evaluation, School of Pharmaceutical Sciences, Sun Yat-sen University, Guangzhou, 510006, China

Received July 08, 2021; Revised March 27, 2022; Editorial Decision March 28, 2022; Accepted March 29, 2022

ABSTRACT

Ligand-Induced duplex-quadruplex transition within the *c-MYC* promoter region is one of the most studied and advanced ideas for *c-MYC* regulation. Despite its importance, there is a lack of methods for monitoring such process in cells, hindering a better understanding of the essence of *c-MYC* G-quadruplex as a drug target. Here we developed a new fluorescent probe ISCH-MYC for specific *c-MYC* G-quadruplex recognition based on GTFH (G-quadruplex-Triggered Fluorogenic Hybridization) strategy. We validated that ISCH-MYC displayed distinct fluorescence enhancement upon binding to *c-MYC* G-quadruplex, which allowed the duplex-quadruplex transition detection of *c-MYC* G-rich DNA in cells. Using ISCH-MYC, we successfully characterized the induction of duplex to G-quadruplex transition in the presence of G-quadruplex stabilizing ligand PDS and further monitored and evaluated the altered interactions of relevant transcription factors Sp1 and CNBP with *c-MYC* G-rich DNA. Thus, our study provides a visualization strategy to explore the mechanism of G-quadruplex stabilizing ligand action on *c-MYC* G-rich DNA and relevant proteins, thereby empowering future drug discovery efforts targeting G-quadruplexes.

INTRODUCTION

G-quadruplexes (G4s) are non-canonical nucleic acid structures formed in guanine-rich (G-rich) DNA or RNA sequences (1,2). Adjacent guanines in G-rich sequence can form G-quartets through Hoogsteen hydrogen bonds. At the same time, the stacking of G-quartets consequently assembles G-quadruplex with a monovalent cation in structure centers such as K^+ or Na^+ (3). Up to date, a flurry of evidence has proven the existence of G-quadruplexes in vitro and in vivo (4–7). According to sequencing analysis, more than 700,000 sequences possess the potential to form G-quadruplexes in human genome (8), noting that G-quadruplexes are widespread in human cells. These potential G-quadruplex sequences were found highly abundant at telomeric ends and oncogenic promoters such as *c-MYC* (9), *c-KIT* (10), *KRAS* (11), *BCL-2* (12) and *VEGF* (13). Recent studies have given sufficient evidence suggesting a relevance between G-quadruplex formation and multiple biological processes such as telomere extension and gene expression regulation, including replication, transcription and translation, demonstrating that G-quadruplexes located in promoters are considered potential regulatory elements in oncogene expression (1,14).

Among all the potential G-quadruplex sequences in human oncogene, *c-MYC* G-quadruplex is one of the most studied sequences due to the common overexpression of *c-MYC* genes in multiple carcinomas such as colorectal, breast, cervix, lung, osteosarcomas and glioblastomas cancers (15,16). c-MYC protein is among the most widespread factors involved in multiple regulatory pathways such as NF-κB and ARF (17), consequently acting as essential regulators of cell proliferation, apoptosis and differentiation. However, c-MYC protein lacking an effective binding site and its extremely short lifetime of 20–30 minutes cause obstacles for it to become a druggable target (18). Inhibiting its upstream gene expression such as transcription is therefore considered an alternative strategy (19,20). It is reported that 85–90% of *c-MYC* transcription activation is controlled by the upstream P1 promoter, which contains the nuclease hypersensitivity element III_1 (NHE III_1) with a 27 base-pairs long G-rich sequence (Pu27) that is capable of engaging in an equilibrium between canonical DNA duplex and G-quadruplex structure (21). Recent studies have suggested that this transition of duplex-quadruplex is essential in *c-MYC* transcription initial procession (9,22). During the transcription initiation, transcription factor Sp1

*To whom correspondence should be addressed. Tel: +86 20 39943053; Email: tanjiah@mail.sysu.edu.cn
Correspondence may also be addressed to Shuo-Bin Chen. Email: chenshb8@mail.sysu.edu.cn

would be recruited to NHE III_1 and unwind the double-stranded structure to initiate transcription (23). As the single-stranded DNA is liberated, G-quadruplex can come into formation and is hypothesized to block the binding of RNA polymerase, leading to transcription stalling. To ensure the transcription ongoing, CNBP protein may bind with the released G-rich region, bearing the function of G-quadruplex helicase and blocking the formation of secondary structure to activate transcription start (24). Based on the close relation of CNBP and Sp1 with G-quadruplex, it is considerably promising to interfere *c-MYC* transcription through stabilizing *c-MYC* G-quadruplex and then altering relevant *c-MYC* DNA-protein interactions during duplex-quadruplex transition (25–27).

Recent studies have further verified the addition of G-quadruplex-stabilizing ligands could cause chances of down-regulating oncogene expression (28–31). In recent years, numerous small molecules targeting *c-MYC* G-quadruplex have been developed due to the repression element role of *c-MYC* G-quadruplex in cancer cells (32–35). Those ligands that are able to induce and stabilize *c-MYC* G-quadruplex have been proven to hold suppression effect on *c-MYC* expression in cell or animal assays, such as TMPyP4 (36) and PDS (Pyridostatin) (37). The binding, inducing and stabilizing abilities of small molecules to *c-MYC* G-quadruplex have been examined through FRET, CD and SPR in vitro (38–40), and the expression regulation effect verified by luciferase reporter assays (41). However, it remains elusive about how ligands interact with *c-MYC* G-quadruplex and induce duplex-quadruplex transition in cells. Additionally, the distribution of G-quadruplexes can be tracked in cells using immunofluorescence antibodies such as BG4 (42) and D1 (43), and an increment of signals could be observed after incubation with G-quadruplex ligands, indicative of their G-quadruplex inducing and stabilizing effects. However, explicitly studying the interactions of *c-MYC* G-quadruplex with small molecules remains challenging due to the lack of strategies for individual DNA G-quadruplex detection.

Previously we have developed GTFH (G-quadruplex-Triggered Fluorogenic Hybridization) strategy to detect specific RNA G-quadruplexes in cells (44). GTFH probes comprise two different moieties: one is the antisense oligonucleotide that complements a sequence adjacent to the G-rich sequence of interest; while the other is a fluorescent 'on-off' switchable chemosensor ISCH, which can emit enhanced fluorescence upon binding with G-quadruplex structures (45). Upon the hybridization of GTFH probes, the complementary binding would have ISCH approaching particular G-rich moiety, consequently realizing the recognition and detection of specific G-quadruplex structure. Enlightened by this idea, we here managed to develop a new GTFH probe **ISCH-MYC** detecting *c-MYC* G-quadruplex in cells and establish novel methods to visualize the *c-MYC* duplex-quadruplex transition and to study the G-quadruplex-small molecule interactions. The fluorescence emission of **ISCH-MYC** would be 'turn-on' when specifically recognizing *c-MYC* G-quadruplex, and 'turn-off' after *c-MYC* G-rich sequence forming duplex structure with its complementary strand. Utilizing a transfected exogenous double-stranded DNA model, the *c-MYC* duplex-quadruplex transition triggered by small-molecule PDS could be visualized under microscopy. We also observed the functions of relevant *c-MYC* transcription factors Sp1 and CNBP hindered during this duplex-quadruplex transition. Our results provide a new strategy to monitor the mechanism of G-quadruplex stabilizing ligand affecting *c-MYC* G-rich DNA along with relevant proteins, and thus advanced the feasibility of intervening *c-MYC* DNA function through small molecules.

MATERIAL AND METHODS

Oligonucleotides, antibodies, G-quadruplex-stabilizing ligands and GTFH probes

The oligonucleotides used in this study are shown in Figure 1A. All DNA oligonucleotides were purchased from Sangon Biotech and Invitrogen. Antibodies for Sp1 and CNBP were purchased from Absin and Invitrogen, respectively. G-quadruplex-stabilizing ligand PDS were purchased from Topscience. GTFH probe was synthesized according to Supplementary Scheme S1. The preparation of ISCH-oa1 was introduced in the previously published article (44). GTFH probe products were further purified with water/acetonitrile on the C18 column and determined by mass spectrometry. The PDS analogue, PDS-A, was synthesized according to Supplementary Scheme S2.

Fluorescence studies

Fluorescence studies were performed on Fluoromax-4 Spectrofluorometer (HORIBA). A quartz cuvette with 2 mm × 10 mm path length was used for the spectra recorded at 1 nm excitation and emission slit widths unless otherwise specified. All DNA oligonucleotides were diluted from stock to final concentration (2 μM) in 10 mM Tris-HCl buffer (100 mM KCl, pH 7.2) containing **ISCH-MYC** at different concentrations. For double-stranded Pu27T/Py27 preparation, additional complementary DNA oligonucleotides Py27 (6 μM) were added to the Pu27T sample. All samples were prepared through heating at 95°C for 5 min followed by slow cooling. The fluorescence spectra in the range of 640–800 nm were recorded when excited at 630 nm.

Immunofluorescence and hybridization experiments in cells (Lipofectamine 3000 as transfection reagent)

The HeLa cells were grown in MEM media containing 10% fetal bovine serum at 37°C, with a 5% CO_2 atmosphere. Cells were seeded in glass-bottom 96-well plate (MatTek) and grew overnight. DNA transfections were performed using 10 pmol DNA oligonucleotides and Lipofectamine 3000 Transfection Reagent (Invitrogen) for over 3 h. This medium was removed after the DNA transfection was completed. For PDS or PDS-A treatment, cells were further incubated in MEM media containing PDS or PDS-A at the certain concentration (10 μM) for 24 h. For fixation, cells were treated with 4% paraformaldehyde in DEPC-PBS at room temperature for 15 min. After rinsing with DEPC-PBS, cells were permeabilized in 0.5% TritonX100/DEPC/PBS at 37°C for 30 min. After rinsing

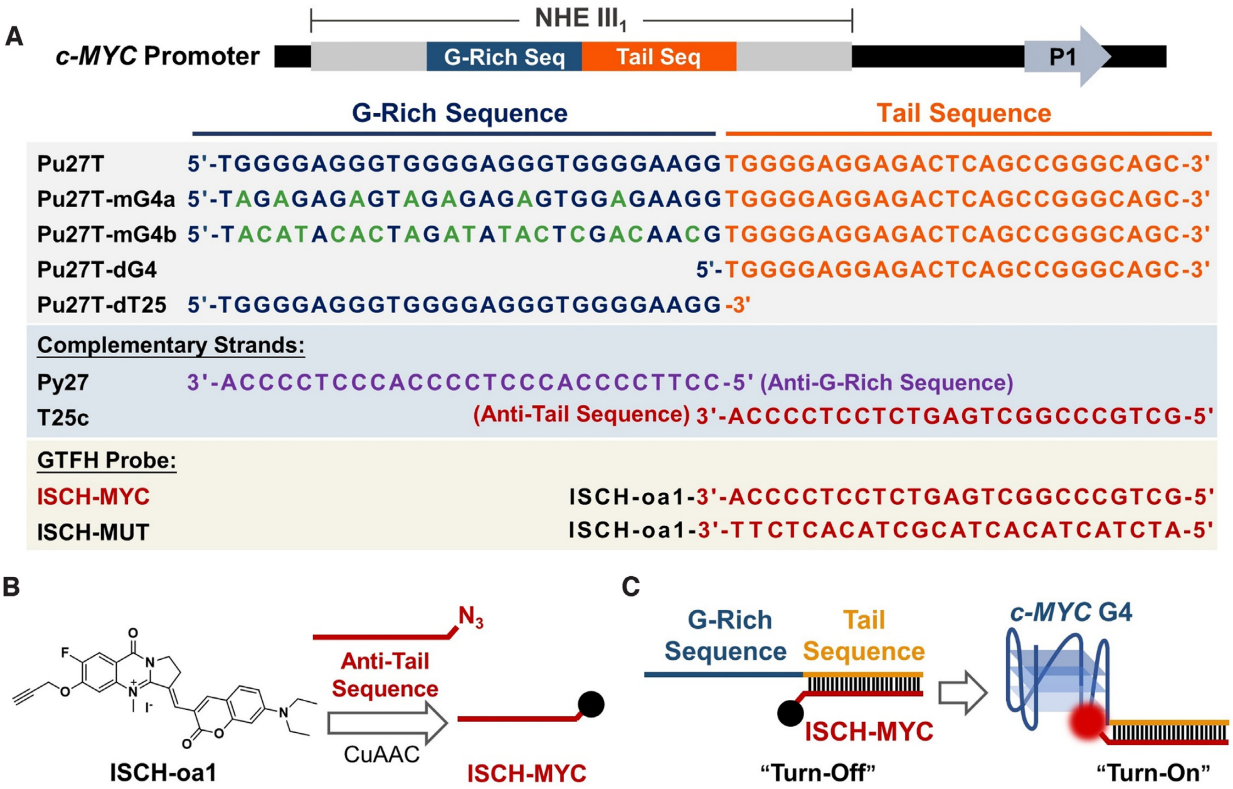

Figure 1. Illustration of GTFH probe **ISCH-MYC** for *c-MYC* G-quadruplex detection. (**A**) *c-MYC* G-rich DNA sequences, complementary sequences and GTFH probes used in this study. (**B**) Synthesis of **ISCH-MYC**. (**C**) Design principle of **ISCH-MYC**.

with 2 × SSC, probes were diluted at 0.3 μM in hybridization buffer (4 × SSC, 0.5 mM EDTA, 10% dextran sulfate, 30% deionized-formamide in DEPC-H_2O) and applied to the cells. Hybridization was done at 37°C overnight. After hybridization, cells were washed in 2 × SSC for 15 min twice and subsequently stained with (0.5 μg·mL^{-1}) DAPI for 15 min. For immunofluorescence, cells were blocked with 3% BSA/PBS at 37°C for 60 min. Next, cells were incubated with Sp1 or CNBP antibody at 4°C overnight and then incubated with Alexa 405-conjugated antibody (A31553, Thermo Fisher Scientific) at 37°C for 1 h. Digital images were recorded using an FV3000 laser scanning confocal microscopy (Olympus) with a 60 × objective lens. The images were analyzed with Imaris software (Bitplane Corp.).

Immunofluorescence and hybridization experiments in cells (Streptolysin O as transfection reagent)

The HeLa cells were grown in MEM media containing 10% fetal bovine serum at 37°C, with a 5% CO_2 atmosphere. Cells were seeded in glass-bottom 96-well plate (MatTek) and grew overnight. Before transfection, cells were treated with 10 μg·mL^{-1} Streptolysin O (abcam) incubation in 1mM $MgCl_2$ for 15 min at 37°C. DNA transfections were performed using 3 μM DNA oligonucleotides in 1 mM $MgCl_2$ buffer with persistent shaking at 37°C. This buffer was removed after the DNA transfection was completed. After transfection, cells were further resealed with 1 mM $CaCl_2$ for 30 min at 4°C. For PDS or PDS-A treatment, cells were further incubated in MEM media containing PDS or PDS-A at the certain concentration (10 μM) for 3 h. For fixation, cells were treated with 4% paraformaldehyde in DEPC-PBS at room temperature for 15 min. After rinsing with DEPC-PBS, cells were permeabilized in 0.5% TritonX100/DEPC/PBS at 37°C for 30 min. After rinsing with 2 × SSC, probes were diluted at 0.3 μM in hybridization buffer (4 × SSC, 0.5 mM EDTA, 10% dextran sulfate, 30% deionized-formamide in DEPC-H_2O) and applied to the cells. Hybridization was done at 37°C overnight. After hybridization, cells were washed in 2 × SSC for 15 min twice and subsequently stained with (0.5 μg·mL^{-1}) DAPI for 15 min. For immunofluorescence, cells were blocked with 3% BSA/PBS at 37°C for 60 min. Next, cells were incubated with Sp1 or CNBP antibody at 4°C overnight and then incubated with Alexa 405-conjugated antibody (A31553, Thermo Fisher Scientific) at 37°C for 1 h. Digital images were recorded using an FV3000 laser scanning confocal microscopy (Olympus) with a 60 × objective lens. The images were analyzed with Imaris software (Bitplane Corp.).

RESULTS

Design and characterization of ISCH-MYC as a *c-MYC* G-quadruplex-specific fluorescent probe in vitro

c-MYC G-quadruplex is a repressive transcription element formed by a 27 bp G-rich sequence in NHE III_1 region. In order to design a GTFH probe specifically recognizing the *c-MYC* G-quadruplex structure, the 25-mer long sequence next to Pu27 was marked as 'Tail Sequence' for hy-

bridization (Figure 1A). *c-MYC* GTFH probe **ISCH-MYC** was synthesized through CuAAC reaction using alkynyl-modified ISCH fluorophore ISCH-oa1 with azido-modified oligonucleotide, a 27 bases long sequence that complements with 'Tail Sequence' (Figure 1B and Supplementary Scheme S1). Based on the GTFH strategy, the complementary binding of this 'Anti-Tail Sequence' moiety would drive ISCH fluorophore to Pu27 sequence and 'turn on' the **ISCH-MYC** with fluorescence enhancement upon recognizing the *c-MYC* G-quadruplex structure (Figure 1C). In addition to **ISCH-MYC**, we also designed and synthetized its negative reference ISCH-MUT whose 'Anti-Tail Sequence' was mutated (Supplementary Scheme S1, Figures S1 and S2).

The binding and selectivity of **ISCH-MYC** to *c-MYC* G-quadruplex DNA were first examined using spectroscopic assays in vitro. DNA sequences investigated in this study are shown in Figure 1A. The native *c-MYC* oligonucleotide Pu27T consisting of a G-rich moiety for G-quadruplex folding and a 'Tail Sequence' moiety for **ISCH-MYC** binding was chosen as the target. In addition, G-rich DNA sequences with mutations (Pu27T-mG4a and Pu27T-mG4b) and deletions (Pu27T-dG4), as well as the tail-deleted sequence (Pu27T-dT25), were applied for controls. These oligonucleotides were then examined by CD, TDS and EMSA studies (46–48). As expected, only Pu27T and Pu27T-dT25 were found to form parallel G-quadruplexes in G-rich moieties. They both showed a significant positive peak at around 265 nm along with a negative peak at around 240 nm in the CD spectra, and a significant positive peak at around 273 nm along with a negative peak at around 295 nm in the TDS spectra (Supplementary Figures S3 and S4). Moreover, Pu27T, Pu27T-mG4a, Pu27T-mG4b and Pu27T-dG4 could hybridize with T25c through the tail sequence (Supplementary Figure S5).

According to the fluorescence results shown in Figure 2A, **ISCH-MYC** alone displayed weak fluorescence emission at the excitation of 630 nm in K^+ buffer. However, a significant fluorescence enhancement near 650 nm was triggered upon the addition of Pu27T. In contrast, no enhancement or even a reduction occurred with the addition of Pu27T-mG4a, Pu27T-mG4b and Pu27T-dG4 variants due to the loss of *c-MYC* G-quadruplex. Likewise, tail-deleted variant Pu27T-dT25 showed little enhancement due to the lack of 'Tail Sequence' for hybridization. Moreover, in the control experiments, negligible fluorescence enhancement was observed upon addition of Pu27T into the negative reference ISCH-MUT, while precursor fluorophore ISCH-oa1 triggered enhancement with Pu27T and Pu27T-dT25 (Supplementary Figure S6). These results suggested the critical function of 'Anti-Tail Sequence' to the selectivity.

Additionally, we found the fluorescence intensity of **ISCH-MYC** with Pu27T gradually enhanced as the concentration of Pu27T increased (Figure 2B), suggesting the fluorescence enhancement of **ISCH-MYC** caused by G-quadruplex was concentration-dependent. We also examined the fluorescence of **ISCH-MYC** in a LiCl buffer (Figure 2C), and observed a remarkable decrease of fluorescence intensity due to the dissociation of G-quadruplex structure by Li^+ (49,50). Moreover, **ISCH-MYC** was also found to show preferential selectivity to *c-MYC* G-quadruplex over other G-quadruplexes such as HRAS, KRAS and HTG48 (Figure 2D). All these results demonstrated the good performance of **ISCH-MYC** as a *c-MYC* G-quadruplex-specific fluorescent probe in vitro.

Characterization of ISCH-MYC as a *c-MYC* G-quadruplex-specific fluorescent probe in cells

Encouraged by the in vitro results, we expected the **ISCH-MYC** available for specific *c-MYC* G-quadruplex detection in cell circumstances as well. However, it is challenging to directly detect single copy of genes such as *c-MYC* under the optical microscopy. Therefore, exogenous DNA transfection to construct intracellular models would be needed for further visualization research in cells. Here we first managed to increase the copy numbers of *c-MYC* G-rich DNA for intracellular visualization using conventional Lipofectamine-based transfection. In addition, to monitor the intracellular distribution of transfected DNA, DNA oligonucleotide was modified with a fluorescein (FAM) label at 3′-end (Figure 3A).

Images were acquired under confocal microscopy after DNAs were transfected into HeLa cells and stained with **ISCH-MYC**. As shown in Figure 3B, the majority of introduced DNAs by Lipofectamine 3000 were located in cytoplasm. **ISCH-MYC** exhibited strong fluorescent foci colocalized with the FAM signals from the transfected Pu27T oligonucleotides. Conversely, little to no foci were observed upon the transfection of 'G-rich Sequence' mutated (Pu27T-mG4a, Pu27T-mG4b), 'G-rich Sequence' deleted (Pu27T-dG4) and 'Tail Sequence' deleted (Pu27T-dT25) variants. These observations were consistent with in vitro spectroscopic results, suggesting that **ISCH-MYC** could also specifically recognize and detect *c-MYC* G-quadruplex in cells. In addition, we applied the precursor fluorophore ISCH-oa1, and negative reference ISCH-MUT to stain Pu27T transfected HeLa cells for comparison. The fluorescence emission of ISCH-oa1 or ISCH-MUT was remarkably weaker than **ISCH-MYC** as neither of them could hybridize with the 'Tail Sequence' of Pu27T (Supplementary Figure S7).

These results have demonstrated the capability of **ISCH-MYC** distinguishing *c-MYC* G-quadruplex in cells using conventional Lipofectamine-based transfection. Most of the oligonucleotides were limited in cytoplasm in this case, while the native *c-MYC* DNA is supposed to be in nucleus. To better understand the nature of *c-MYC* G-rich DNA, we intended to deliver the oligonucleotides into cell nucleus. After trying various ways of transfection, we finally succeeded in nuclear delivery using Streptolysin O. Streptolysin O is a membrane-poring toxin that enables highly efficient and reversible membrane permeabilization, and exogenous biomolecules exchanges (51). In Streptolysin O-permeabilized HeLa cells, **ISCH-MYC** foci displayed strong colocalization with FAM signals of Pu27T oligonucleotides in the nucleus, while no signals from **ISCH-MYC** were observed in the case of other variants transfection. (Figure 3C). These results were consistent with the observations in cell cytoplasm, demonstrating that the **ISCH-MYC** was able to specifically detect *c-MYC* G-quadruplex in cells.

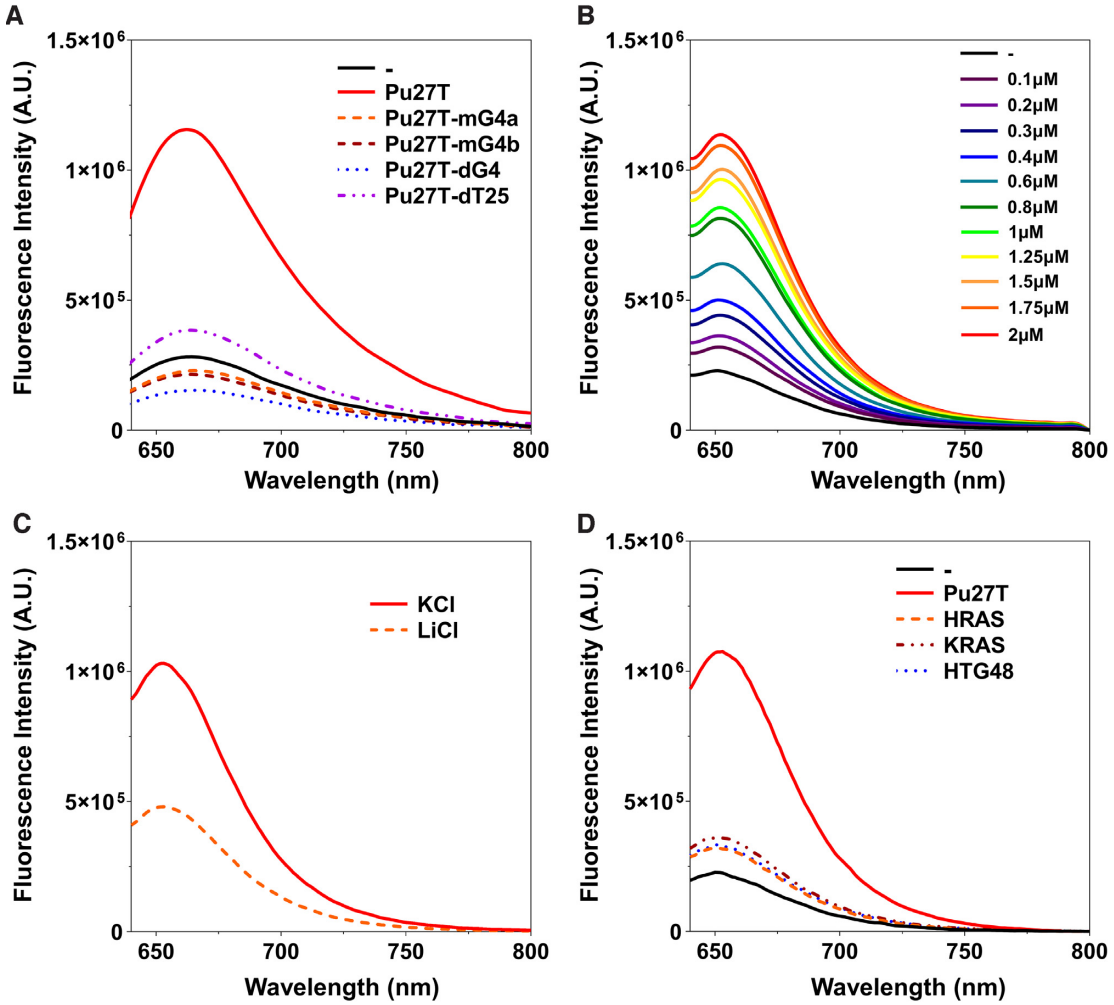

Figure 2. Fluorescence spectra of **ISCH-MYC** with DNAs. (**A**) Fluorescence spectra of 1 μM **ISCH-MYC** with or without 2 μM DNAs in 10 mM Tris-HCl buffer, 100 mM KCl, pH 7.2. (**B**) Fluorescence spectra of 1 μM **ISCH-MYC** with Pu27T of different concentrations in 10 mM Tris-HCl buffer, 100 mM KCl, pH 7.2. (**C**) Fluorescence spectra of 1 μM **ISCH-MYC** with 2 μM Pu27T in 10 mM Tris-HCl buffer, pH 7.2 containing 100 mM KCl or LiCl. (**D**) Fluorescence spectra of 1 μM **ISCH-MYC** with or without 2 μM DNA G-quadruplexes in 10 mM Tris-HCl buffer, 100 mM KCl, pH 7.2.

Visualization of ligand-induced *c-MYC* duplex–quadruplex transition

As is mentioned above, the transition of double-stranded DNA to G-quadruplex in NHE III_1 essentially functions as a regulator in *c-MYC* transcription process. However, little is known about the *c-MYC* duplex-quadruplex transition occurrence in cells heretofore. As **ISCH-MYC** specifically recognizing *c-MYC* G-quadruplex was validated, we further intended to explore its application of visualizing *c-MYC* duplex-quadruplex transition in cells. To achieve this, we established a double-stranded *c-MYC* G-rich DNA model for this study. We complemented the 'G-rich Sequence' moiety of Pu27T with the antisense oligonucleotide Py27 to form duplex structure. The 'Tail Sequence' moiety, however, remained accessible for **ISCH-MYC** hybridization. We assumed that **ISCH-MYC** fluorescence would be 'turn-off' when Pu27T/Py27 remained in duplex status, while 'turn-on' once transited into G-quadruplex structure (Figure 4A). As expected, **ISCH-MYC** fluorescence remarkably decreased after the double-stranded Pu27T/Py27 was formed in vitro (Supplementary Figures S8 and S9). Similar intracellular results were observed in double-stranded Pu27T/Py27 transfected cells. We noticed the **ISCH-MYC** fluorescence in both the cytoplasm and the nucleus mostly disappeared, showing the signals were 'turn-off' when G-quadruplex was transited into duplex form (Figure 4B and C).

Next, as the capacity of **ISCH-MYC** detecting the transition of *c-MYC* G-rich DNA from G-quadruplex to duplex has been confirmed, we expected that **ISCH-MYC** could also be applied to visualize the G-quadruplex forming from duplex induced by small molecules. Here we focused on one of the most studied G-quadruplex ligand PDS, which has been reported as a highly selective ligand stabilizing G-quadruplex structures (52). As for comparison, an analogue of PDS (namely PDS-A) was designed and synthesized to be lack of G-quadruplex-stabilizing function (Supplementary Scheme S2 and Figure S10). The stabilizing effects of PDS and PDS-A to *c-MYC* G-quadruplex were validated by CD melting studies (Supplementary Figure S11). The

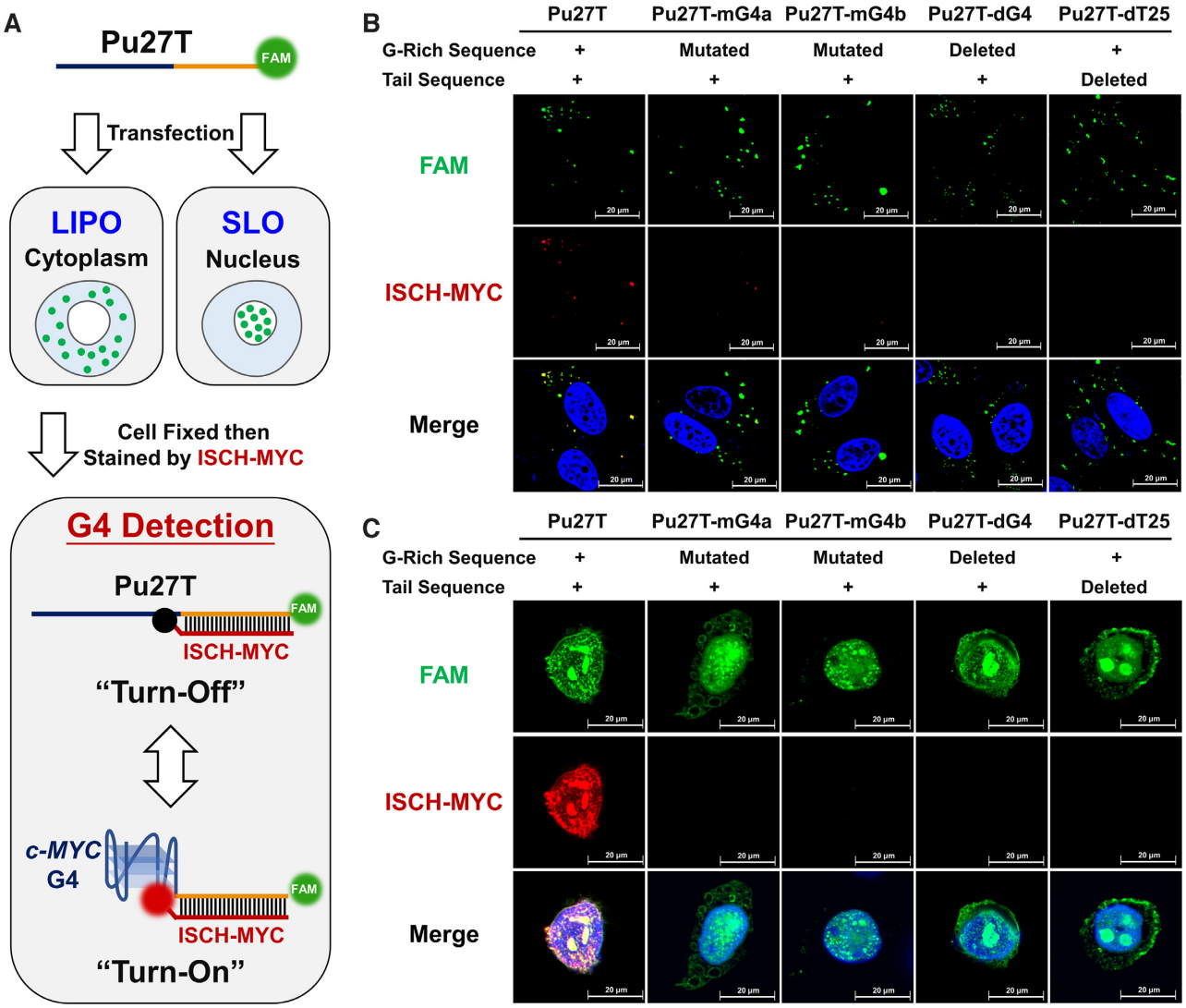

Figure 3. Confocal imaging of FAM-labeled DNA-transfected cells stained by **ISCH-MYC**. (**A**) Schematic diagram of cell imaging process using Lipofectamine 3000 (LIPO) or Streptolysin O (SLO) as transfection reagent. (**B**) Imaging of FAM-labeled DNA-transfected cells stained by **ISCH-MYC**. The DNAs are delivered into cytoplasm by Lipofectamine 3000. (**C**) Imaging of FAM-labeled DNA-transfected cells stained by **ISCH-MYC**. The DNAs are delivered into nucleus by Streptolysin O.

melting temperature difference between PDS and PDS-A treatment demonstrated that PDS could bind to and stabilize *c-MYC* G-quadruplex while PDS-A could not. Consistent with this, PDS treatment could further lead to the dissociation of double-stranded Pu27T/Py27 and formation of a G-quadruplex structure in vitro as determined by EMSA and fluorescence studies (Supplementary Figures S8 and S12). Notably, we found that detection of *c-MYC* G-quadruplex using **ISCH-MYC** was not affected by the addition of PDS (Supplementary Figure S13). This finding was similar to the previous results obtained on PDS and ISCH fluorophore (53), suggesting their cooperative binding to G-quadruplex structure. On the other hand, PDS displayed little cytotoxicity to HeLa cells as the IC_{50} value was above 25 μM (Supplementary Figure S14). It was also noteworthy that treatments of cells with PDS or PDS-A in our experiments may not interfere the transfection of *c-MYC* G-rich DNA, because they were performed after the complete removal of medium containing Lipofectamine 3000/Streptolysin O and oligonucleotides (Supplementary Figure S15).

Encouraged by these results, we applied PDS on the double-stranded Pu27T/Py27 transfected cells. As shown in Figure 4B and C, we observed the previously quenched fluorescence of **ISCH-MYC** in cytoplasm and nucleus partially reappeared upon PDS treatment, suggesting that PDS treatment induced the transition of *c-MYC* G-rich DNA from duplex to G-quadruplex. Conversely, little signal reappearance was observed with PDS-A treatment. In addition, quantification of the enhancement of **ISCH-MYC** fluorescence in Pu27T/Py27 transfected cells treated with PDS in different concentrations and different durations were conducted. We found that the reappeared fluorescence was PDS concentration-dependent as well as time-dependent

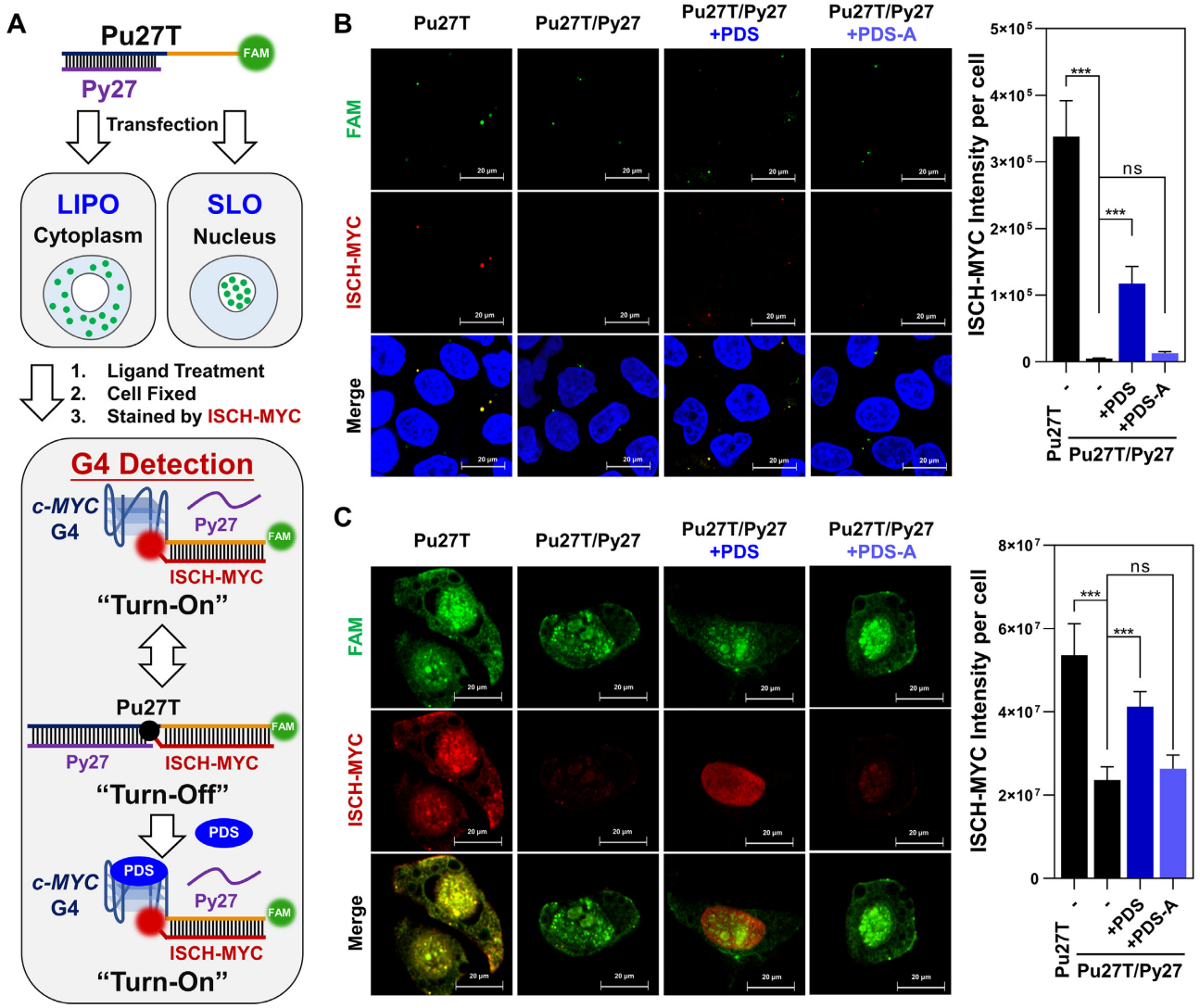

Figure 4. Detection of ligand-induced duplex-quadruplex transition in cells. (**A**) Schematic diagram of cell imaging process using Lipofectamine 3000 (LIPO) or Streptolysin O (SLO) as transfection reagent. (**B**) Imaging of *c-MYC* G-rich DNA-transfected cells treated with PDS or PDS-A then stained by **ISCH-MYC**. The DNAs are delivered into cytoplasm by Lipofectamine 3000. (**C**) Imaging of *c-MYC* G-rich DNA-transfected cells treated with PDS or PDS-A then stained by **ISCH-MYC**. The DNAs are delivered into nucleus by Streptolysin O. Quantification of fluorescence was shown on the right. Quantification data are expressed as the mean ± SEM (standard error of mean). For each sample, about 100 cells were measured. The standard error was calculated from a set of three replicate experiments. Statistical significance was determined by the *t* test as (ns) not significant, (*) $P < 0.05$, (**) $P < 0.01$, and (***) $P < 0.001$.

(Supplementary Figure S16). Taken together, these results confirmed that **ISCH-MYC** was able to be utilized for visualizing the *c-MYC* duplex-quadruplex transition induced by small molecules in cells.

Visualization of the altered distribution of Sp1 and CNBP upon PDS-induced *c-MYC* duplex–quadruplex transition

As mentioned above, multiple proteins function in duplex-quadruplex transition during the transcription process. Encouraged by the successful visualization of *c-MYC* duplex-quadruplex transition in cells, we expected that **ISCH-MYC** could also be applied for studying the behaviors of relevant proteins when interfered during this transition. Here we focused on the transcription factors Sp1 and CNBP, which act as double-stranded unwinder and G-quadruplex forming repressor respectively. We intended to visualize their distribution variation and study their interactions with the *c-MYC* G-rich DNA during duplex-quadruplex transition process.

Immunofluorescence was applied to track the distribution of Sp1 and CNBP in cells. Secondary antibodies were labeled with the cyan dye AlexaFluor 405, while Pu27T oligonucleotide was labeled with green fluorophore FAM. Because Sp1 and CNBP were reported to be localized in both cytoplasm and nucleus (54,55), we investigated *c-MYC* DNA-protein interactions in cells using Lipofectamine 3000 and Streptolysin O as transfection reagents, respectively. In the initial phase (Figure 5A), Sp1 was supposed to interact with double-stranded NHE III1 region to

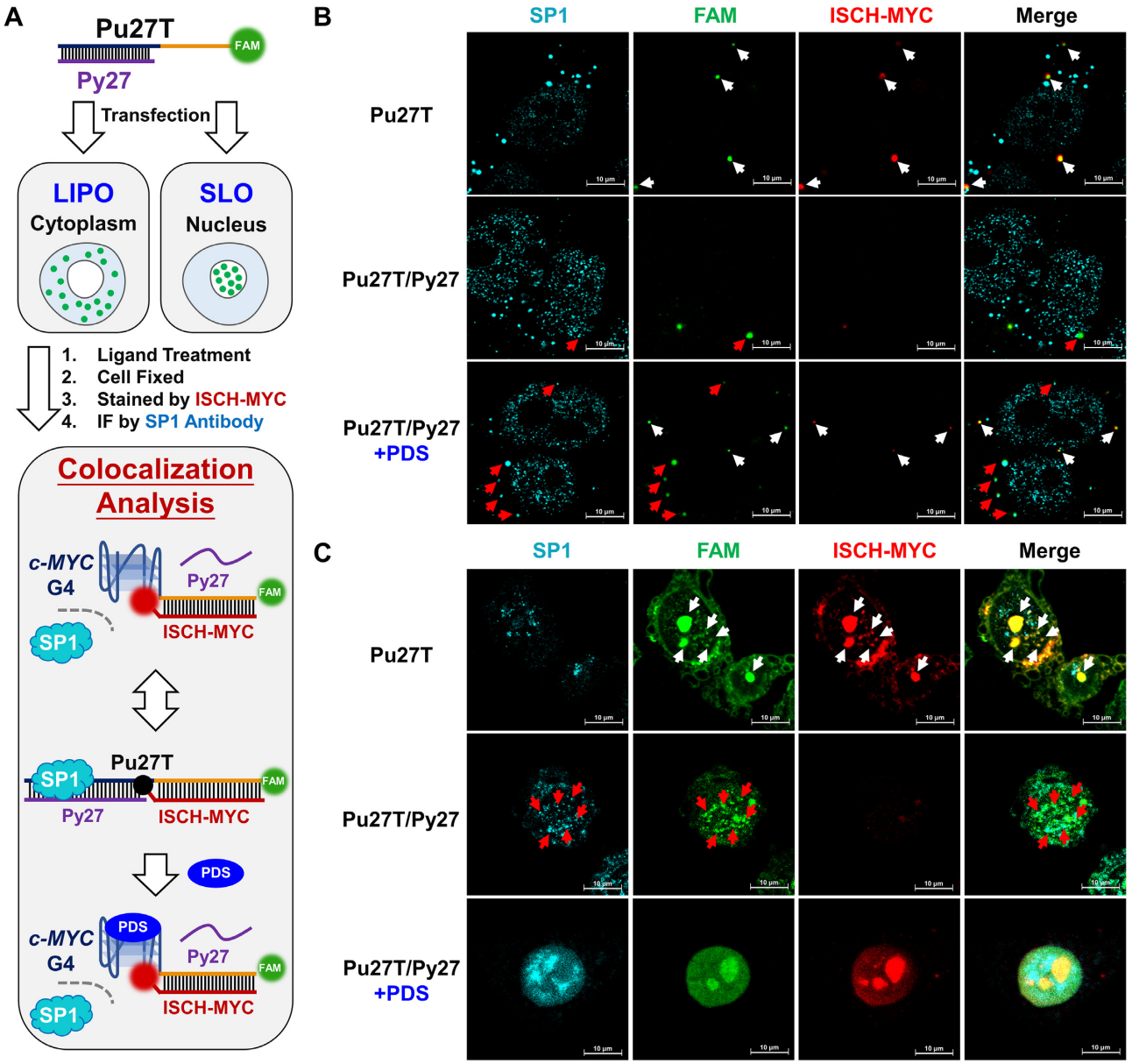

Figure 5. Visualization of the altered *c-MYC* DNA-Sp1 interactions. (**A**) Schematic diagram of cell imaging and analysis process using Lipofectamine 3000 (LIPO) or Streptolysin O (SLO) as transfection reagent. (**B**) Immunofluorescence imaging of Sp1 in Pu27T or Pu27T/Py27 transfected cells treated with or without PDS then stained by **ISCH-MYC**. The DNAs are delivered into cytoplasm by Lipofectamine 3000. (**C**) Immunofluorescence imaging of Sp1 in Pu27T or Pu27T/Py27 transfected cells treated with or without PDS then stained by **ISCH-MYC**. The DNAs are delivered into nucleus by Streptolysin O. White arrows indicate the distinct colocalization of FAM foci with 'turn-on' **ISCH-MYC** signals; while red arrows indicate the distinct colocalization of FAM foci with Sp1 signals (**ISCH-MYC** signals were 'turn-off' in this case).

open double-stranded structure for initial preparation, consequently releasing the G-rich single strand that would fold into a G-quadruplex structure and stall the transcription (23). Therefore, we expected that the Sp1 would colocalize with transfected double-stranded Pu27T/Py27 DNA but not with Pu27T G-quadruplex DNA. According to Figure 5, in both cases of cytoplasm and nucleus, there was no colocalization of Sp1 with *c-MYC* G-quadruplex upon single-stranded Pu27T transfection (overlapped FAM and **ISCH-MYC** signals were shown in white arrows), while a portion of Sp1 signals colocalized with FAM-labeled double-stranded Pu27T/Py27 DNA (shown in red arrows, **ISCH-MYC** signals were 'turn-off' in this case).

Interestingly, in PDS-treated Pu27T/Py27 transfected cells using Lipofectamine 3000 as transfection reagent, two different signal distributions were observed under confocal imaging in cytoplasm (Figure 5B). We observed a portion of FAM signals had the same distributions as in Pu27T transfected cells, colocalizing with **ISCH-MYC** but not with Sp1 signals (shown in white arrows), while other foci remained colocalized with Sp1 (shown in red arrows), suggesting the successful formation of G-quadruplexes induced by PDS

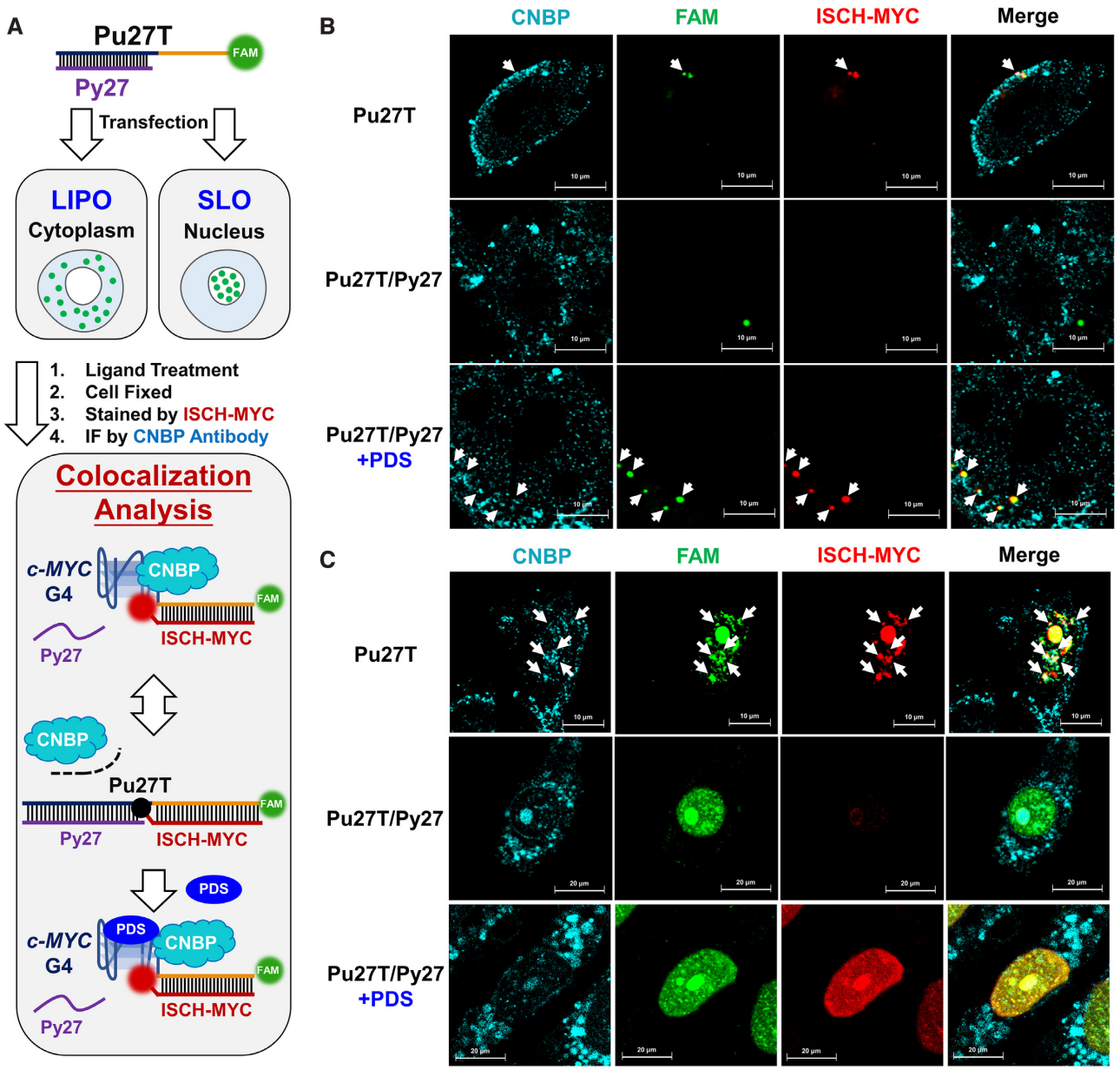

Figure 6. Visualization of the altered *c-MYC* DNA-CNBP interactions. (**A**) Schematic diagram of cell imaging and analysis process using Lipofectamine 3000 (LIPO) or Streptolysin O (SLO) as transfection reagent. (**B**) Immunofluorescence imaging of CNBP in Pu27T or Pu27T/Py27 transfected cells treated with or without PDS then stained by **ISCH-MYC**. The DNAs are delivered into cytoplasm by Lipofectamine 3000. (**C**) Immunofluorescence imaging of CNBP in Pu27T or Pu27T/Py27 transfected cells treated with or without PDS then stained by **ISCH-MYC**. The DNAs are delivered into nucleus by Streptolysin O. White arrows indicate the distinct colocalization of FAM foci, CNBP foci and 'turn-on' **ISCH-MYC** signals.

blocked Sp1 from interacting with duplex DNA. Similarly, in the case of transfection using Streptolysin O, we observed the overlapping fluorescence for FAM-labeled DNA and **ISCH-MYC** (Figure 5C). However, these signals were distributed diffusely and uniformly over the nucleus. This might be due to the redistribution of high-concentration oligonucleotides when PDS induced the formation of *c-MYC* G-quadruplex. Although it seemed that there was no significant colocalization of Sp1 and **ISCH-MYC**, it was still very difficult to accurately study the colocalization of Sp1 with different DNAs in this case. Despite this, our overall findings provided new evidence to support previous idea that addition of a G-quadruplex stabilizer may suspend the processing of *c-MYC* transcription by forming quadruplex blockage preventing interactions of Sp1 with duplex.

On the other hand, CNBP would be recruited to the G-rich moiety to prevent the G-quadruplex formation and ensure the ongoing process of transcription (Figure 6A). Additionally, CNBP has also been reported bearing functions as G-quadruplex helicase (24). Consistent with this idea, CNBP immunofluorescence results displayed a different colocalization pattern as compared with Sp1. According to Figure 6, in both cases of cytoplasm and nucleus, CNBP foci could be observed colocalized with the FAM-

labeled Pu27T and **ISCH-MYC** in Pu27T transfected cells without PDS treatment (shown in white arrows), suggesting the recruitment of CNBP to *c-MYC* G-quadruplex. While in double-stranded Pu27T/Py27 transfected cells, the colocalization of CNBP with FAM signals became lost, showing that CNBP was unable to interact with *c-MYC* G-rich DNA upon the G-quadruplex transited into the duplex (**ISCH-MYC** signals were 'turn-off' in this case). However, in PDS-treated Pu27T/Py27 transfected cells using Lipofectamine 3000 as transfection reagent, CNBP foci colocalized with reappeared **ISCH-MYC** foci again in cytoplasm (Figure 6B). These results implied that CNBP might function as a quadruplex helicase that can be recruited to G-quadruplex structure to ensure the ongoing transcription. Nevertheless, the existence of PDS would stabilize the G-quadruplex structure and prevent G-quadruplex from being disassembled by CNBP, consequently blocking the initial of *c-MYC* transcription. It was also noteworthy that, in the case of transfection using Streptolysin O, although it seemed that there was some colocalization of CNBP and **ISCH-MYC** in PDS-treated cells, diffuse FAM-labeled DNA and **ISCH-MYC** fluorescence made it difficult to exactly investigate their colocalization with CNBP (Figure 6C).

Collectively, using **ISCH-MYC** along with immunofluorescence staining, we were able to visualize different *c-MYC* DNA-protein interactions upon duplex-quadruplex transition to some extent. We observed Sp1 being recruited to double-stranded *c-MYC* DNA and blocked away when duplex transited into G-quadruplex. In the case of CNBP, we also observed the recruitment of CNBP to G-quadruplex. These results were consistent with the previously described potential functions of Sp1/CNBP on *c-MYC* DNA. Conclusively, our studies described a feasible method for visualizing the *c-MYC* duplex-quadruplex transition, whose occurrence might alter the interactions between *c-MYC* DNA and relevant proteins in cells. In virtue of the direct visualization by **ISCH-MYC**, our method could potentially be utilized for further studying the mechanism of *c-MYC* transcription.

DISCUSSION

This study synthesized a new fluorescence probe **ISCH-MYC** specifically recognizing *c-MYC* G-quadruplex based on the GTFH strategy. We verified the fluorescence features of **ISCH-MYC** to find the probe able to trigger fluorescence enhancement upon specifically recognizing *c-MYC* G-quadruplex. On this basis, we established a method for previously intractable *c-MYC* duplex-quadruplex transition detection in cells. We observed the **ISCH-MYC** fluorescence signals were 'turn-off' with *c-MYC* G-quadruplex transited into the double-stranded status, and 'turn-on' again upon small molecule ligands inducing the transition of the *c-MYC* duplex to G-quadruplex. Further studies revealed that this *c-MYC* duplex-quadruplex transition could alter the distribution of relevant transcription factors Sp1 and CNBP, proving small molecules stabilizing G-quadruplex could hinder the interactions of transcription factors with *c-MYC* G-rich DNA during transcription process. However, few questions remained yet to be solved. For example, our study was obliged to apply exogenous model transfection instead of in situ detection due to the inability to detect a single copy of *c-MYC* gene in cells. Moreover, the current GTFH strategy is mainly based on in situ hybridizations in fixed cells, limiting the further application for dynamic duplex-quadruplex transition imaging in live cells. These questions are still awaited to be conquered by the optimized GTFH strategy in the future.

Nevertheless, our results have shown G-quadruplex stabilizing ligand could induce *c-MYC* duplex-quadruplex transition and might further alter the interactions between Sp1/CNBP and *c-MYC* G-rich DNA in cells. These findings may provide new evidence and insights for small molecules interfering *c-MYC* transcription. Moreover, with the help of **ISCH-MYC**, it is possible to establish a fluorescent screening platform in search of *c-MYC* G-quadruplex ligands as promising drug candidates. Taken together, our study offers a potent method for visualizing the *c-MYC* duplex-quadruplex transition and relevant interactions of *c-MYC* DNA with proteins under the effects of G-quadruplex stabilizing ligands. It expanded the understanding of the roles of small molecules involved in *c-MYC* transcription inhibition, contributing to further development of new drugs and therapies targeting *c-MYC* G-quadruplex DNA.

DATA AVAILABILITY

All data produced or analyzed for this study are available from the corresponding author upon request.

SUPPLEMENTARY DATA

Supplementary Data are available at NAR Online.

FUNDING

This work was supported by the National Key Research and Development Program (No. 2017YFE0109900), the National Natural Science Foundation of China (Nos. 21977124, 81973184 and 81930098), the Fundamental Research Funds for the Central Universities (20ykzd16), the Guangdong Provincial Key Laboratory of Construction Foundation (No. 2020B1212060034), the Outstanding Talents of Guangdong Special Plan (No. 2019JC05Y456) and the Chang Jiang Scholars Program.
Conflict of interest statement. None declared.

REFERENCES

1. Varshney,D., Spiegel,J., Zyner,K., Tannahill,D. and Balasubramanian,S. (2020) The regulation and functions of DNA and RNA G-quadruplexes. *Nat. Rev. Mol. Cell. Biol.*, **21**, 459–474.
2. King,J.J., Irving,K.L., Evans,C.W., Chikhale,R.V., Becker,R., Morris,C.J., Pena Martinez,C.D., Schofield,P., Christ,D., Hurley,L.H. *et al.* (2020) DNA G-quadruplex and i-Motif structure formation is interdependent in human cells. *J. Am. Chem. Soc.*, **142**, 20600–20604.
3. Burge,S., Parkinson,G.N., Hazel,P., Todd,A.K. and Neidle,S. (2006) Quadruplex DNA: sequence, topology and structure. *Nucleic Acids Res.*, **34**, 5402–5415.
4. Wu,F., Niu,K.K., Cui,Y., Li,C.C., Lyu,M., Ren,Y.D., Chen,Y.F., Deng,H.M., Huang,L.H., Zheng,S.C. *et al.* (2021) Genome-wide analysis of DNA G-quadruplex motifs across 37 species provides insights into G4 evolution. *Commun. Biol.*, **4**, 98.
5. Zyner,K.G., Mulhearn,D.S., Adhikari,S., Martinez Cuesta,S., Di Antonio,M., Erard,N., Hannon,G.J., Tannahill,D. and

Balasubramanian,S. (2019) Genetic interactions of G-quadruplexes in humans. *Elife*, **8**, e46793.
6. Marsico,G., Chambers,V.S., Sahakyan,A.B., McCauley,P., Boutell,J.M., Antonio,M.D. and Balasubramanian,S. (2019) Whole genome experimental maps of DNA G-quadruplexes in multiple species. *Nucleic Acids Res.*, **47**, 3862–3874.
7. Salgado,G.F., Cazenave,C., Kerkour,A. and Mergny,J.L. (2015) G-quadruplex DNA and ligand interaction in living cells using NMR spectroscopy. *Chem. Sci.*, **6**, 3314–3320.
8. Chambers,V.S., Marsico,G., Boutell,J.M., Di Antonio,M., Smith,G.P. and Balasubramanian,S. (2015) High-throughput sequencing of DNA G-quadruplex structures in the human genome. *Nat. Biotechnol.*, **33**, 877–881.
9. Chaudhuri,R., Bhattacharya,S., Dash,J. and Bhattacharya,S. (2021) Recent update on targeting c-MYC G-quadruplexes by small molecules for anticancer therapeutics. *J. Med. Chem.*, **64**, 42–70.
10. Wei,D., Husby,J. and Neidle,S. (2015) Flexibility and structural conservation in a c-KIT G-quadruplex. *Nucleic Acids Res.*, **43**, 629–644.
11. Ou,A., Schmidberger,J.W., Wilson,K.A., Evans,C.W., Hargreaves,J.A., Grigg,M., O'Mara,M.L., Iyer,K.S., Bond,C.S. and Smith,N.M. (2020) High resolution crystal structure of a KRAS promoter G-quadruplex reveals a dimer with extensive poly-A π-stacking interactions for small-molecule recognition. *Nucleic Acids Res.*, **48**, 5766–5776.
12. Agrawal,P., Lin,C., Mathad,R.I., Carver,M. and Yang,D. (2014) The major G-quadruplex formed in the human BCL-2 proximal promoter adopts a parallel structure with a 13-nt loop in K^+ solution. *J. Am. Chem. Soc.*, **136**, 1750–1753.
13. Agrawal,P., Hatzakis,E., Guo,K., Carver,M. and Yang,D. (2013) Solution structure of the major G-quadruplex formed in the human VEGF promoter in K^+: insights into loop interactions of the parallel G-quadruplexes. *Nucleic Acids Res.*, **41**, 10584–10592.
14. Spiegel,J., Adhikari,S. and Balasubramanian,S. (2020) The structure and function of DNA G-quadruplexes. *Trends Chem.*, **2**, 123–136.
15. Balasubramanian,S., Hurley,L.H. and Neidle,S. (2011) Targeting G-quadruplexes in gene promoters: a novel anticancer strategy? *Nat. Rev. Drug Discovery*, **10**, 261–275.
16. Hansel-Hertsch,R., Simeone,A., Shea,A., Hui,W.W.I., Zyner,K.G., Marsico,G., Rueda,O.M., Bruna,A., Martin,A., Zhang,X. *et al.* (2020) Landscape of G-quadruplex DNA structural regions in breast cancer. *Nat. Genet.*, **52**, 878–883.
17. Chen,H., Liu,H.D. and Qing,G.L. (2018) Targeting oncogenic myc as a strategy for cancer treatment. *Signal Transduct. Target. Ther.*, **3**, 5.
18. Brooks,T.A. and Hurley,L.H. (2009) The role of supercoiling in transcriptional control of MYC and its importance in molecular therapeutics. *Nat. Rev. Cancer*, **9**, 849–861.
19. Neidle,S. (2016) Quadruplex nucleic acids as novel therapeutic targets. *J. Med. Chem.*, **59**, 5987–6011.
20. Brooks,T.A. and Hurley,L.H. (2010) Targeting MYC expression through G-quadruplexes. *Genes Cancer*, **1**, 641–649.
21. Gonzalez,V. and Hurley,L.H. (2010) The c-MYC NHE III_1: function and regulation. *Annu. Rev. Pharmacol. Toxicol.*, **50**, 111–129.
22. Endo,M., Xing,X., Zhou,X., Emura,T., Hidaka,K., Tuesuwan,B. and Sugiyama,H. (2015) Single-Molecule manipulation of the duplex formation and dissociation at the G-quadruplex/i-Motif site in the DNA nanostructure. *ACS Nano*, **9**, 9922–9929.
23. Parisi,F., Wirapati,P. and Naef,F. (2007) Identifying synergistic regulation involving c-Myc and sp1 in human tissues. *Nucleic Acids Res.*, **35**, 1098–1107.
24. David,A.P., Pipier,A., Pascutti,F., Binolfi,A., Weiner,A.M.J., Challier,E., Heckel,S., Calsou,P., Gomez,D., Calcaterra,N.B. *et al.* (2019) CNBP controls transcription by unfolding DNA G-quadruplex structures. *Nucleic Acids Res.*, **47**, 7901–7913.
25. Balaratnam,S. and Schneekloth,J.S. (2020), Transcriptional regulation of MYC through G-quadruplex structures. In: Neidle,S. (ed). *Quadruplex Nucleic Acids As Targets For Medicinal Chemistry*. Academic Press, Cambridge, pp. 361–407.
26. Carvalho,J., Mergny,J.L., Salgado,G.F., Queiroz,J.A. and Cruz,C. (2020) G-quadruplex, friend or foe: the role of the G-quartet in anticancer strategies. *Trends Mol. Med.*, **26**, 848–861.
27. Brown,R.V., Danford,F.L., Gokhale,V., Hurley,L.H. and Brooks,T.A. (2011) Demonstration that drug-targeted down-regulation of MYC in non-hodgkins lymphoma is directly mediated through the promoter G-quadruplex. *J. Biol. Chem.*, **286**, 41018–41027.
28. Wang,K.B., Elsayed,M.S.A., Wu,G., Deng,N., Cushman,M. and Yang,D. (2019) Indenoisoquinoline topoisomerase inhibitors strongly bind and stabilize the MYC promoter G-quadruplex and downregulate MYC. *J. Am. Chem. Soc.*, **141**, 11059–11070.
29. Calabrese David,R., Hewitt William,M., Alden,S., Hilimire Thomas,A., Saunders Lindsey,B., Schneekloth John,S. Jr, Chen,X., He,F., Walters Kylie,J., Leon Elena,C. *et al.* (2018) Chemical and structural studies provide a mechanistic basis for recognition of the MYC G-quadruplex. *Nat. Commun.*, **9**, 4229.
30. Das,R.N., Chevret,E., Desplat,V., Rubio,S., Mergny,J.L. and Guillon,J. (2018) Design, synthesis and biological evaluation of new substituted diquinolinyl-pyridine ligands as anticancer agents by targeting G-quadruplex. *Molecules*, **23**, 81.
31. Kawauchi,K., Sugimoto,W., Yasui,T., Murata,K., Itoh,K., Takagi,K., Tsuruoka,T., Akamatsu,K., Miyoshi,D., Tateishi-Karimata,H. *et al.* (2018) An anionic phthalocyanine decreases NRAS expression by breaking down its RNA G-quadruplex. *Nat. Commun.*, **9**, 2271.
32. Dickerhoff,J., Dai,J. and Yang,D. (2021) Structural recognition of the MYC promoter G-quadruplex by a quinoline derivative: insights into molecular targeting of parallel G-quadruplexes. *Nucleic Acids Res.*, **49**, 5905–5915.
33. Boddupally,P.V., Hahn,S., Beman,C., De,B., Brooks,T.A., Gokhale,V. and Hurley,L.H. (2012) Anticancer activity and cellular repression of c-MYC by the G-quadruplex-stabilizing 11-piperazinylquindoline is not dependent on direct targeting of the G-quadruplex in the c-MYC promoter. *J. Med. Chem.*, **55**, 6076–6086.
34. Ji,X., Sun,H., Zhou,H., Xiang,J., Tang,Y. and Zhao,C. (2012) The interaction of telomeric DNA and C-myc22 G-quadruplex with 11 natural alkaloids. *Nucleic Acid Ther.*, **22**, 127–136.
35. Phan,A.T., Kuryavyi,V., Gaw,H.Y. and Patel,D.J. (2005) Small-molecule interaction with a five-guanine-tract G-quadruplex structure from the human MYC promoter. *Nat. Chem. Biol.*, **1**, 167–173.
36. Le,H.T., Miller,M.C., Buscaglia,R., Dean,W.L., Holt,P.A., Chaires,J.B. and Trent,J.O. (2012) Not all G-quadruplexes are created equally: an investigation of the structural polymorphism of the c-Myc G-quadruplex-forming sequence and its interaction with the porphyrin TMPyP4. *Org. Biomol. Chem.*, **10**, 9393–9404.
37. Di Antonio,M., McLuckie,K.I. and Balasubramanian,S. (2014) Reprogramming the mechanism of action of chlorambucil by coupling to a G-quadruplex ligand. *J. Am. Chem. Soc.*, **136**, 5860–5863.
38. Tran,P.L.T., Rieu,M., Hodeib,S., Joubert,A., Ouellet,J., Alberti,P., Bugaut,A., Allemand,J.F., Boule,J.B. and Croquette,V. (2021) Folding and persistence times of intramolecular G-quadruplexes transiently embedded in a DNA duplex. *Nucleic Acids Res.*, **49**, 5189–5201.
39. Renciuk,D., Zhou,J., Beaurepaire,L., Guedin,A., Bourdoncle,A. and Mergny,J.-L. (2012) A FRET-based screening assay for nucleic acid ligands. *Methods*, **57**, 122–128.
40. Zhang,Z., He,X. and Yuan,G. (2011) Regulation of the equilibrium between G-quadruplex and duplex DNA in promoter of human c-myc oncogene by a pyrene derivative. *Int. J. Biol. Macromol.*, **49**, 1173–1176.
41. Halder,K., Benzler,M. and Hartig,J.S. (2012) Reporter assays for studying quadruplex nucleic acids. *Methods*, **57**, 115–121.
42. Biffi,G., Tannahill,D., McCafferty,J. and Balasubramanian,S. (2013) Quantitative visualization of DNA G-quadruplex structures in human cells. *Nat. Chem.*, **5**, 182–186.
43. Liu,H.-Y., Zhao,Q., Zhang,T.-P., Wu,Y., Xiong,Y.-X., Wang,S.-K., Ge,Y.-L., He,J.-H., Lv,P., Ou,T.-M. *et al.* (2016) Conformation selective antibody enables genome profiling and leads to discovery of parallel G-quadruplex in human telomeres. *Cell Chem. Biol.*, **23**, 1261–1270.
44. Chen,S.-B., Hu,M.-H., Liu,G.-C., Wang,J., Ou,T.-M., Gu,L.-Q., Huang,Z.-S. and Tan,J.-H. (2016) Visualization of NRAS RNA G-quadruplex structures in cells with an engineered fluorogenic hybridization probe. *J. Am. Chem. Soc.*, **138**, 10382–10385.
45. Yan,J.-W., Chen,S.-B., Liu,H.-Y., Ye,W.-J., Ou,T.-M., Tan,J.-H., Li,D., Gu,L.-Q. and Huang,Z.-S. (2014) Development of a new colorimetric and red-emitting fluorescent dual probe for G-quadruplex nucleic acids. *Chem. Commun.*, **50**, 6927–6930.

46. Kypr,J., Kejnovska,I., Renciuk,D. and Vorlickova,M. (2009) Circular dichroism and conformational polymorphism of DNA. *Nucleic Acids Res.*, **37**, 1713–1725.
47. Sun,D. and Hurley,L.H. (2010) Biochemical techniques for the characterization of G-quadruplex structures: EMSA, DMS footprinting, and DNA polymerase stop assay. *Methods Mol. Biol.*, **608**, 65–79.
48. Mergny,J.L., Li,J., Lacroix,L., Amrane,S. and Chaires,J.B. (2005) Thermal difference spectra: a specific signature for nucleic acid structures. *Nucleic Acids Res.*, **33**, e138.
49. Smargiasso,N., Rosu,F., Hsia,W., Colson,P., Baker,E.S., Bowers,M.T., De Pauw,E. and Gabelica,V. (2008) G-quadruplex DNA assemblies: loop length, cation identity, and multimer formation. *J. Am. Chem. Soc.*, **130**, 10208–10216.
50. Lyu,K., Chen,S.-B., Chan,C.-Y., Tan,J.-H. and Kwok,C.K. (2019) Structural analysis and cellular visualization of APP RNA G-quadruplex. *Chem. Sci.*, **10**, 11095–11102.
51. Bao,H.-L., Liu,H.-s. and Xu,Y. (2019) Hybrid-type and two-tetrad antiparallel telomere DNA G-quadruplex structures in living human cells. *Nucleic Acids Res.*, **47**, 4940–4947.
52. Rodriguez,R., Miller,K.M., Forment,J.V., Bradshaw,C.R., Nikan,M., Britton,S., Oelschlaegel,T., Xhemalce,B., Balasubramanian,S. and Jackson,S.P. (2012) Small-molecule-induced DNA damage identifies alternative DNA structures in human genes. *Nat. Chem. Biol.*, **8**, 301–310.
53. Chen,X.-C., Tang,G.-X., Luo,W.-H., Shao,W., Dai,J., Zeng,S.-T., Huang,Z.-S., Chen,S.-B. and Tan,J.-H. (2021) Monitoring and modulating mtDNA G-quadruplex dynamics reveal its close relationship to cell glycolysis. *J. Am. Chem. Soc.*, **143**, 20779–20791.
54. Zhao,Q., Cai,W., Zhang,X., Tian,S., Zhang,J., Li,H., Hou,C., Ma,X., Chen,H., Huang,B. *et al.* (2017) RYBP expression is regulated by KLF4 and Sp1 and is related to hepatocellular carcinoma prognosis. *J. Biol. Chem.*, **292**, 2143–2158.
55. Armas,P., Coux,G., Weiner Andrea,M.J. and Calcaterra Nora,B. (2021) What's new about CNBP? Divergent functions and activities for a conserved nucleic acid binding protein. *Biochim. Biophys. Acta, Gen. Subj.*, **1865**, 129996.